Interacting Lattice Gas Automaton Study of Liquid-Gas Properties in Porous Media

V. Pot, C. Appert, A. Melayah, D. Rothman, Stéphane Zaleski

J. Phys. II France 6 (1996) 1517–1534 OCTOBER 1996, PAGE 1517

Interacting Lattice Gas Automaton Study of Liquid-Gas Properties in Porous Media

V. Pot ([1,*]), C. Appert ([2]), A. Melayah ([3]), D.H. Rothman ([4]) and S. Zaleski ([5])

([1]) Laboratoire de Biogéochimie Isotopique ([**]), Université Pierre et Marie Curie - INRA, Tour 26, case 120, 4 place Jussieu, 75252 Paris Cedex 05, France et
Laboratoire de Géologie Appliquée, CNRS, Université Pierre et Marie Curie, 75252 Paris Cedex 05, France
([2])Laboratoire de Physique Statistique, École Normale Supérieure, CNRS, 24 rue Lhomond, 75231 Paris Cedex 05, France
([3]) INRA, Station de Science du Sol d'Avignon, B.P. 91, 84143 Montfavet Cedex, France
([4])Department of Earth, Atmospheric and Planetary Sciences, M.I.T., Cambridge, Ma 02139, USA
([5]) Laboratoire de Modélisation en Mécanique, CNRS, Tour 66, Université Pierre et Marie Curie, 75252 Paris Cedex 05, France

(Received 19 July 1995, revised 17 April 1996, accepted 13 June 1996)

PACS.47.55.Kf – Multiphase and particle-laden flows
PACS.47.55.Mh – Flows through porous media
PACS.92.40.Je – Evaporation

Abstract. — We describe how lattice-gas cellular automata may be used to simulate evaporation phenomena in models of porous media constructed at the pore scale. Two-dimensional simulations of evaporation are performed in simple channel geometries and in a model of a microscopically disordered porous medium. We describe a variant of the lattice gas, called the liquid-gas model. By static and dynamic tests we show that this model can simulate low Reynolds number mechanical and thermodynamical equations for isothermal evaporation in a real system made of a single-species liquid in equilibrium with its vapor. From static simulations in simple geometries we obtain equilibrium pressures on both sides of a meniscus. These are seen to obey the Gibbs-Thomson relations, which are equivalent to the Kelvin effect. We observe evaporation in simple capillary channels and compare the results to a simple theory based on Poiseuille flow. An unexpected effect is additional flow in the wetting films and sharp density jumps. In simulations of evaporation in disordered geometries, we observe bursting and convoluted interfaces as previously reported in laboratory experiments.

Résumé. — Nous décrivons comment un automate cellulaire, le gaz sur réseau, peut être utilisé pour simuler les phénomènes d'évaporation dans des modèles de milieux poreux construits à l'échelle du pore. Des simulations bi-dimensionnelles d'évaporation sont réalisées dans la géométrie simple du tube et dans un modèle de milieu poreux microscopiquement désordonné. Nous décrivons une variante du gaz sur réseau, appelé le modèle liquide-gaz. À l'aide de tests statiques et dynamiques, nous montrons que ce modèle peut simuler les équations mécaniques et thermodynamiques à faible nombre de Reynolds, pour une évaporation isotherme dans un système réel composé d'une espèce unique sous forme liquide en équilibre avec sa vapeur. À partir

([*]) Author for correspondence (e-mail: pot@ccr.jussieu.fr)
([**]) UMR 162 CNRS

des simulations statiques dans des géométries simples, nous obtenons les pressions d'équilibre de part et d'autre d'un ménisque. Celles-ci obéissent aux relations de Gibbs-Thomson, relations équivalentes à l'effet Kelvin. Nous observons une évaporation dans des tubes capillaires et comparons les résultats à une théorie simple basée sur le flux de Poiseuille. Un effet inattendu est un flux additionnel dans les films mouillants et de brusques sauts de densité. Dans les simulations d'évaporation en géométries désordonnées, nous observons des avancées par sauts et des interfaces irrégulières, comme déja décrites dans les expériences en laboratoire.

1. Introduction

The invasion of one fluid into a porous medium filled by another fluid presents problems of both practical and fundamental interest [1–3]. Within just the earth sciences, practical concerns range from problems encountered in secondary oil recovery to the prediction of the spreading of contaminants in groundwater reservoirs. Deeper in the earth, the segregation of melt from partially molten mantle rock may be viewed as a problem of multiphase flow in porous media [4]. Because of the intricate, and often fractal, patterns formed by the invading front, the general problem is considered one of the simplest examples of pattern formation in nonequilibrium fluids [5].

Theoretical, experimental, and numerical studies generally consider the case of two non-reacting, thermodynamically stable fluids such as oil and water. Evaporation in porous rocks is a more complex displacement process that involves a rich microscopic physics. During the process of evaporation or drying of a rock, water is transported from the saturated pore to the outside both in the gas phase present in unsaturated pores and in the liquid phase. It is generally believed that an important fraction of the water passes either through the saturated pores [6] or through thin liquid films present on the sidewalls of the pores [7].

Irregularly shaped fronts are observed in microscopic evaporation experiments [7]. This irregularity may be explained at least in part by capillary effects. Capillary forces play an important role in shaping the liquid-gas interface and determining which pores remain saturated. The large pores offer little resistance to the advance of the meniscus and empty first. Smaller pores remain saturated longer, and may remain saturated when the evaporation front has traversed the box.

Despite the qualitative understanding of the evaporation process, a detailed microscopic description is lacking. For some geometries in the static case, *i.e.* when the effect of fluid motion may be neglected, the shape of interfaces may be found theoretically. For instance in a circular tube the meniscus is a spherical cap. Analytic solutions are however missing beyond such special cases and numerical solutions are required. Interest in the physics of the displacement process at the microscopic pore scale has recently led to the development of new numerical methods [8, 9]. These methods are variations of *lattice-gas automata* [10–14]. Here we show how another lattice-gas automaton, called the liquid-gas model [15, 16] may be used to study evaporation in porous media.

Our purpose in this paper is mainly methodological. We have extended and tested the liquid-gas model to adapt it to porous media simulations. A new feature with respect to previously published work is the presence of "solid sites" allowing the simulation of solid grains in a porous medium. The liquid-gas model has interesting wetting properties in the presence of these solid grains. We first report measurements of these properties and check their consistency against those made in the absence of solid walls by Appert and Zaleski (1993). We also report a simple evaporation experiment in the presence of Poiseuille flow in the gas phase, allowing us

a comparison with an analytic expression for the evaporating front. Finally we report on more complex evaporation experiments. They illustrate the ability of our model to reproduce some of the microscopic pore-scale features of evaporation.

2. Method

Our approach to modelling involves two conceptual steps. First we simplify the evaporation problem to a one-species, isothermal problem. This simplification is motivated by practical concerns, mostly our limited ability to simulate thermal effects with the lattice gas. Second we use the liquid-gas model to study this simplified problem. The present paper reports our first use of this model with solid walls. To validate our model in the presence of such walls we performed tests of static and dynamical wetting properties, which we report below.

2.1. The Liquid-Gas Lattice Model. — The liquid-gas model is a variant of the lattice-gas cellular automaton of Frisch *et al.* (1986). This liquid-gas model has been defined and studied in several papers [15–18]. We thus describe the model only briefly.

2.1.1. Model Definition. — We consider a 2D lattice gas on a hexagonal lattice as in Figure 1. On each site, there is at most one particle moving in each direction of the lattice and at most one particle at rest. In the classical lattice gas, particles evolve through collisions and propagation to nearest neighbor sites on the lattice. A detailed description of the model can be found in [11, 14].

In the liquid-gas model, interactions between distant pairs of sites are used in addition to the classical collisions. The interaction range is a fixed number r. In the applications reported in this paper we use $r = 3$ sites. Interactions act like van der Waals forces in a real fluid and lead to a liquid-gas transition. The liquid-gas model has thus two coexisting phases of high and low density. The extension of the liquid-gas interface is of the order of the interaction range, namely 2 or $3r$. Here we use two variants of the liquid-gas model called Model A and Model C. In Model A, interactions are performed independently of the number of particles in the interacting sites. In Model C, interactions are performed only if the number of particles is larger than 4. This results in different physical characteristics of the two models as reported in Table I. In particular, Model C has a higher gas density. The reason for introducing several different models is principally to avoid some difficulties appearing in the simple evaporation experiments of Section 2.4. A detailed description of the liquid-gas model and of its variants is given in [16].

Solid sites are added to the model used in this work. As in the classical lattice gas, particles bounce back on these sites. This means that during the collision step they simply return to the site they were coming from. Thus a particle cannot enter a region of the lattice filled with solid sites.

Particles on the non-solid sites are also attracted by solid sites. This is performed by adding to the particle some momentum oriented towards the solid site. This solid-particle interaction has the same range r as the ordinary interaction. The strength of the solid-particle interaction is tuned by controlling the amount of momentum that can be added to the particle. The amount by which momentum can change can never be greater than a number g_w. This affords us a crude way of controlling wetting. More refined ways would include a different range for the solid-particle interactions and probabilistic ways to control the amount of momentum change. In most experiments reported in this paper we used $g_w = 2$.

2.1.2. Hydrodynamical Equations. — The hydrodynamical equations of a two phase system can be decomposed into bulk equations, jump conditions on the interfaces, and boundary

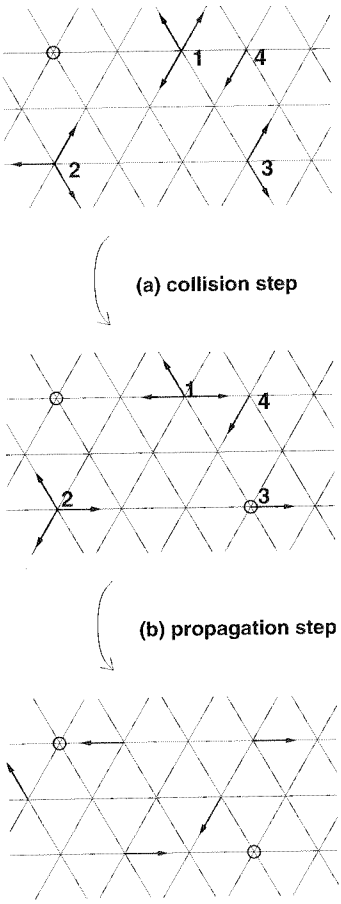

Fig. 1. — Propagation and collision on a hexagonal lattice. (a) Particles are represented before their collisions and after. Small circles represent particles at rest, with 0 momentum. Labels 1 and 2 refer respectively to two- and three-body collisions. Label 3 shows a collision involving a rest particle, and label 4 a particle not involved in the collision step. Notice that each collision conserves total momentum. Some sites are left unchanged as there is no possible redistribution of particles that conserves momentum. (b) Propagation of particles is shown. Each particle advances by one step in the direction of its momentum.

conditions. The bulk equations for the lattice liquid-gas model are derived in [16]. They are valid on the *hydrodynamical scale* which is defined as a scale much larger than the mean free path of the particles. In the low Reynolds and Mach number limit they simplify to

$$\partial_t \rho \mathbf{u} = -\nabla p + \nabla \mathbf{S}, \tag{1}$$

where $\mathbf{S}$ is the usual viscous stress tensor:

$$S_{ij} = \eta \left(\frac{\partial u_j}{\partial x_i} + \frac{\partial u_i}{\partial x_j} \right). \tag{2}$$

and η is the dynamic viscosity, related to the kinematic viscosity ν by $\eta = \rho\nu$. The pressure p is related to density ρ by an equation of state $p = p(\rho)$ calculated in [16,17]. Mass conservation

yields

$$\partial_t \rho + \nabla \cdot (\rho \mathbf{u}) = 0. \tag{3}$$

However the model is used only at low Mach numbers $M = |\mathbf{u}|/c_s$ (we note $c_s^2 = \mathrm{d}p/\mathrm{d}\rho$ the sound speed squared). In the limit of vanishing M and in the bulk of each phase we have the incompressibility condition

$$\nabla \cdot \mathbf{u} = 0. \tag{4}$$

On the walls the presence of solid sites implies as for the usual lattice gas the rigid boundary condition $\mathbf{u} = 0$.

Liquid-gas thermodynamical equilibrium is realized for a flat interface at a well-defined pressure P_{eq}. At equilibrium the liquid and gas densities are ρ_{L} and ρ_{G} and verify $P_{\mathrm{eq}} = p(\rho_{\mathrm{L}}) = p(\rho_{\mathrm{G}})$. The values of P_{eq}, ρ and of other relevant parameters of the liquid-gas model have been measured using procedures described in part in [16] and in part in the following Sections of this paper. They are summarized in Table I.

On interfaces there are further, mechanical jump conditions for the flow of mass, the tangential velocities, and the total stresses. We have continuity of the stress tensor [14, 19]:

$$\left[(S_{ij} + p\delta_{ij})\, n_j\right]_{\mathrm{L}} - \left[(S_{ij} + p\delta_{ij})\, n_j\right]_{\mathrm{G}} = \sigma \kappa n_i \tag{5}$$

where $\mathbf{n}$ is the unit vector normal to the interface, κ is the total curvature $1/R_1 + 1/R_2$ and σ is the surface tension. When the viscous stresses can be neglected these conditions amount to the Young-Laplace equation

$$P_{\mathrm{G}} - P_{\mathrm{L}} = \sigma \kappa. \tag{6}$$

The liquid gas model is expected to have complicated and relatively unphysical jump conditions for the tangential velocity $\mathbf{u} \cdot \mathbf{t}$ on the interface [16]. This difficulty may be circumvented for the evaporation problems considered in the present paper. The fact that the liquid is most of the time at rest leads to simplified conditions: near the interface $\mathbf{u}_{\mathrm{L}} = 0$ on the liquid side, while when the interface is approached from the gas side, $\mathbf{u}_{\mathrm{G}} \cdot \mathbf{t} = 0$, where $\mathbf{t}$ is the unit vector tangent to the interface. The normal gas velocity is given by the following expression which expresses the conservation of mass:

$$\rho_{\mathrm{G}} \mathbf{u}_{\mathrm{G}} \cdot \mathbf{n} = (\rho_{\mathrm{G}} - \rho_{\mathrm{L}}) V_{\mathrm{I}}. \tag{7}$$

here V_{I} is the interface velocity.

In addition to these mechanical conditions there are modified thermodynamical conditions in the presence of a curved interface. In the presence of a pressure jump across the interface the equilibrium temperatures and pressures are different from those found for a flat surface and obey the Gibbs-Thomson conditions [20]. For the lattice gas, these conditions were obtained by direct measurements of static droplet pressures reported in [16]. They read

$$\begin{aligned} P_{\mathrm{G}} &= P_{\mathrm{eq}} + (1 - \alpha \frac{\rho_{\mathrm{L}}}{\rho_{\mathrm{L}} - \rho_{\mathrm{G}}}) \sigma \kappa \\ P_{\mathrm{L}} &= P_{\mathrm{eq}} - \alpha \frac{\rho_{\mathrm{L}}}{\rho_{\mathrm{L}} - \rho_{\mathrm{G}}} \sigma \kappa \end{aligned} \tag{8}$$

which is equivalent to

$$\begin{aligned} P_{\mathrm{G}} &= P_{\mathrm{eq}} + (1 - \alpha \frac{\rho_{\mathrm{L}}}{\rho_{\mathrm{L}} - \rho_{\mathrm{G}}})(P_{\mathrm{G}} - P_{\mathrm{L}}) \\ P_{\mathrm{L}} &= P_{\mathrm{eq}} - \alpha \frac{\rho_{\mathrm{L}}}{\rho_{\mathrm{L}} - \rho_{\mathrm{G}}} (P_{\mathrm{G}} - P_{\mathrm{L}}) \end{aligned} \tag{9}$$

where κ is the curvature of the interface and α is a coefficient of proportionality specific to the lattice gas. The typical value of this coefficient is one. In our liquid gas model α equals 1.35. When this coefficient is left arbitrary, equations (8) express the most general form for a dependency of the equilibrium pressure that is *i*) linear in $\sigma\kappa = |P_G - P_L|$ and *ii*) compatible with the Young-Laplace equation. The most important new effect when the isothermal evaporation problem is compared to immiscible displacement is the linear dependence of each equilibrium pressure on $\sigma\kappa$. This is also known as the Kelvin effect. Indeed in immiscible displacement only the pressure difference across the meniscus is given. Fixing the pressure allows in turn to find the pressure gradient in the gas region. This problem is worked out in a simple case in Section 2.4. Tests of the Gibbs-Thomson relations in the presence of solid walls are reported in Section 2.3.

A final hydrodynamical scale condition concerns the contact angle at points where the liquid gas interface meets the walls. On length scales l such that $r \ll l \ll R$ where r is the range of microscopic interactions and R the curvature one should observe a straight interface making an angle θ with the wall. When the contact angle is not zero the fluid is non-wetting, but even in the non-wetting case there may still be microscopic layers deposited on the solid walls [21].

2.1.3. Scaling. — Following the tradition in lattice-gas studies all units are expressed in lattice-gas units. Thus the separation between sites is one unit of length. The time unit is the time step, and the mass of a particle is the unit of mass. To scale our results, it is convenient to take the typical velocity of the gas U_G as a velocity scale and the typical pore size D as a length scale. If gravity is neglected (a simplifying assumption which will be discussed below) the problem has four dimensionless numbers. The Reynolds number is $\mathrm{Re} = g(\rho_G)\rho_G U_G D/\eta_G$ where η_G is the gas dynamic viscosity and $g(\rho_G)$ is the non-Galilean factor which can be found in [14]. The other dimensionless numbers are the density ratio ρ_L/ρ_G, the viscosity ratio η_L/η_G, and the capillary number $\mathrm{Ca} = \eta_G U_G/\sigma$. The latter number is the most important since it controls the balance between capillary forces and viscous dissipation. In many evaporation experiments it is extremely small. For a 10 cm box evaporating in one day $\mathrm{Ca} \simeq 10^{-7}$. It is impossible to reach such a small capillary number on present day computers with the lattice gas. The capillary numbers obtained in simulations are on the order of $\mathrm{Ca} \simeq 10^{-2}$ and thus much larger than what would be realistic in a natural setting or a laboratory experiment. We do not know whether this difference in capillary numbers would cause qualitative or only quantitative changes in the evaporation process.

2.2. Implementation and Design of Simulations

2.2.1. Implementation. — The liquid-gas model was implemented on Sun Sparc 2, Solbourne and IBM Risc 6000 workstations. Collisions and interactions are performed using look-up tables. A speed of up to 5.6×10^4 sites per second was reached on the Sparc and Solbourne while we reached 2.8×10^5 on the Risc 6000.

2.2.2. Initial and Boundary Conditions. — Simulations were performed in rectangular boxes of width L_x and height L_z. In the tests of this Section simple wall geometries were used. In the next Section we choose a more complex grain geometry. For an initial condition we filled the lattice with liquid. This was performed by putting particles at random on the lattice at a density equal to the equilibrium density of the liquid. This fixed both the density and the pressure, the latter being fixed through the equation of state. The initial gas densities also corresponded to the equilibrium values.

Boundary conditions were periodic in the horizontal direction so that for any quantity A we had $A(x + L_x, z, t) = A(x, z, t)$ at all times t and heights z. This is equivalent to let a particle

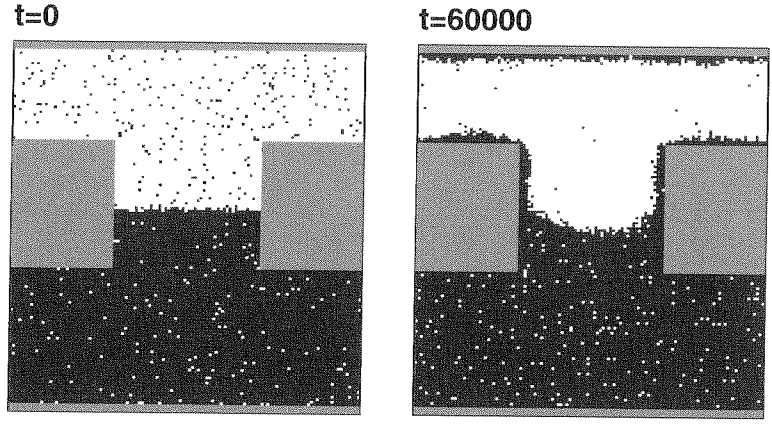

Fig. 2. — A model capillary throat. Grey squares are solid grains. Sites with more than 3 particles are in black while those with less than 3 particles are in white. Thus the mostly black area is liquid while the mostly white area is gas. The density of black or white dots gives an indication of the density of the gas or liquid phase. The system equilibrates from $t = 0$ to about $t = 10000$. During equilibration, thin liquid films form on the grains. The gas density decreases and the liquid density increases to approach the values given in Table I. With appropriately chosen initial conditions, as in this figure, the meniscus stabilizes in the middle of the capillary throat where measurements of capillary effects can be reliably performed. The pressure measurements reported in the text are performed between $t = 30000$ and $t = 60000$. Model A was used with $g_w = 2$.

leaving the box on the left reenter it on the right. On the vertical we placed a rigid wall at the bottom of the box so that $\mathbf{u} = 0$ for $z = 0$. In static experiments (Sect. 2.3) the top also has a closed wall. In dynamic experiments (Sects. 2.4 and 3) density is fixed to some value ρ_1 at the top. When $\rho_1 > 0$ particles were removed *and* added at random on the top layer to satisfy this boundary condition.

2.3. Static Validation. — Capillary properties of the liquid-gas model in presence of walls were tested. A simple capillary throat was constructed with two solid blocks of size $\ell_x \times \ell_z$ with height ℓ_z fixed to 50 lattice sites and variable width ℓ_x. The simulations were performed in boxes containing 144×120 lattice sites, with the boundary conditions of Section 2.2.

The simulation is initialized with liquid filling the bottom part of the box as shown in Figure 2. After an initial transient equilibrium is reached at the hydrodynamical scale. During the transient one can observe *microscopic* liquid films condensing on the solid walls and a meniscus forming in the capillary throat. These microscopic wetting films are of a thickness approaching the range r of the interaction. The final result after equilibration is shown in Figure 2.

The equilibrium pressures are measured far enough from the walls and the interfaces to avoid spurious pressure variations near the interfaces. The resulting pressures are plotted in Figure 3. To compare our measurements to equations (8) we need to estimate the curvature of the meniscus. This was done in the following way.

The equilibrium shape of a meniscus in a throat of width R is that of a circle of radius $R/\cos\theta$ forming a contact point on the wall at an angle θ. This model does not give very good results for small R. Thus we replaced it by a model in which the contact point is located on the edge of a wetting film of thickness e and obtain $\kappa = \cos\theta/(R - e)$. The resulting fit with $e = 3$ sites is shown in Figure 3. We note a deviation from linearity at largest curvatures. In

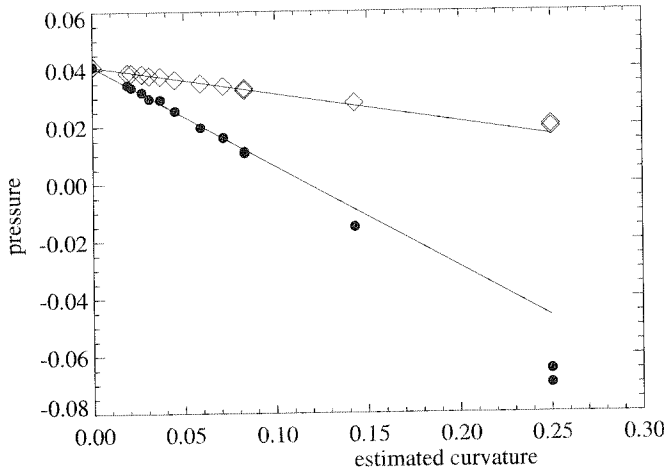

Fig. 3. — Liquid and gas equilibrium pressures as a function of capillary width. Diamonds represent gas pressure and small black dots liquid pressure. The abscissa corresponds to the inverse of the estimated radius of curvature $\kappa = 1/r'$ (see text). The linear relation shows qualitative agreement with the dependence of pressures on curvature predicted by thermodynamics (8).

Table I. — *A summary of model parameters.*

Parameters	Model A	Model C
$P_{\rm eq}(^a)$	0.0426 ± 0.002	0.280 ± 0.004
$d_{\rm G}(^c)$	0.0165 (^{a}) ± 0.001	0.097 ± 0.01
$d_{\rm L}(^c)$	0.575 (^{a}) ± 0.003	0.610 ± 0.002
$\eta_{\rm G}$	0.103 ± 0.01 (^{a})	0.28 (^{b}) ± 0.01
$\eta_{\rm G}(^d)$	–	0.30 ± 0.04
$\eta_{\rm L}(^a)$	3.9 ± 0.6	5.4 ± 0.6
$\sigma(^a)$	0.22 ± 0.02	0.027 ± 0.03
$\cos\theta_0(^{g,e})$	0.969 ± 0.022	0.98 ± 0.04
$\cos\theta_{30}(^{g,f})$	0.966 ± 0.01	0.97 ± 0.015
$\sigma\cos\theta_0(^h)$	0.21 ± 0.02	0.092 ± 0.08
$\sigma\cos\theta_{30}(^h)$	0.3 ± 0.02	0.0724 ± 0.005

(^{a}) From [16]. (^{b}) Obtained using the decaying sine wave method as in [16].
(^{c}) Reduced densities $d = \rho/7$. (^{d}) From Poiseuille flow experiment in Section 2.4.
(^{e}) Contact angle for wall aligned with the lattice.
(^{f}) Contact angle for wall at 30 deg. with the lattice.
(^{g}) From direct fit of the meniscus, see Section 2.3, with $g_{\rm w} = 2$
(^{h}) From static pressure measurements, see Section 2.3, with $g_{\rm w} = 2$.

the limit of small radii we reach microscopic length scales where the approximations leading to Laplace's law cease to be valid. Thus, we may suggest a rule of thumb: one needs to use pore diameters greater than 8 sites in the modelling of a porous medium to avoid the effect of the microscopic forces.

We have also performed direct measurements of the contact angle θ by fitting a circular meniscus shape to the data. Specifically, pressure measurements were performed during the simulations. To decrease the statistical noise a time averaging was performed. Finally the contours of pressures were computed and fit to a circle. The resulting intersection near the wall gives the contact angle with some uncertainty due to the presence of the wetting forces near the wall. The results are shown in Table I.

We have also at our disposal a direct measurement of surface tension from the stress tensor in the lattice gas [16]. The result of that measurement, also shown in Table I, can be cross-checked against the measurements of $\sigma \cos\theta$ and θ reported above. The agreement is good, indicating that our fundamental assumptions about the hydrodynamical scale behavior of the model are correct.

2.4. DYNAMICAL VALIDATION. — In systems away from thermodynamic equilibrium, transport of mass may occur through convection in the liquid phase, convection in the gas phase or both. The viscosity of the liquid phase was measured using a simple Poiseuille flow experiment in [22]. In this section we study the corresponding flow in the gas phase. This brings us two benefits: we check the estimate of viscosity given in [16] and we get a closer look at gas phase transport in a simple capillary. The capillary was modelled by walls parallel to an axis of the lattice. The following conventions are used: depth h is positive downward and the top of the capillary is fixed at depth $h = 0$ (Fig. 4a).

A gas density gradient is performed through the channel: the gas density is fixed as described in Section 2.2 in regions near the top and the bottom of the capillary respectively defined between depths 0 and h_1 ($h_1 > 0$) and between depths $L - h_1$ and L. L is the length of the capillary. The depth h_1, of the order of 10 lattice sites is chosen for technical reasons related to the existence of correlations over distances of the order of the interaction range. Thus unlike the previous experiment the number of particles is not conserved. The density at the top region is set to ρ_1 and at the bottom region to ρ_2. The density ρ_2 is set close to the equilibrium gas density ρ_G, which is attained near a static liquid–gas interface as reported in Section 2.3. The density ρ_1 is set inferior to ρ_G. Model C was used because of its higher gas density and shorter mean free path between particle collisions.

An interesting effect is that this set-up produces an unexpected pair of density jumps at depths h_1 and $L - h_1$ separated by a linear gradient, as clearly seen in Figure 4b. We are unable at present to trace the origin of these jumps. Their effect is seen in other experimental set-ups such as a simple evaporation experiment in a test channel.

The viscosity of the gas phase was measured using the assumption of a uniform Poiseuille flow between the fixed density regions. Its value η_G is given in Table I. The velocity profiles display a transition between Blasius and Poiseuille type profiles at the top and the bottom of the channel, as predicted (at higher Reynolds numbers) in [23, 24]. We checked that these transition regions do not affect the viscosity measurement. We calculated the gas viscosity in the central region of the channel where the velocity profile is close to a Poiseuille type profile as shown by Figure 5. We found $\eta_G = 0.27 \pm 0.01$ very close to the former measurement. Thus, there appears to be very little difference in the pressure drop predicted assuming a uniform Poiseuille flow and obtained by the full simulation. We therefore keep this assumption in our analysis of the evaporation numerical experiment to which we now turn.

In the test evaporation experiment, the capillary was made of parallel walls and is initially partially filled with liquid with the meniscus at a given depth h_0. As before, we imposed the density of the particles in a region near the top to be $\rho_1 < \rho_G$, but there are effects similar to the jumps discussed above.

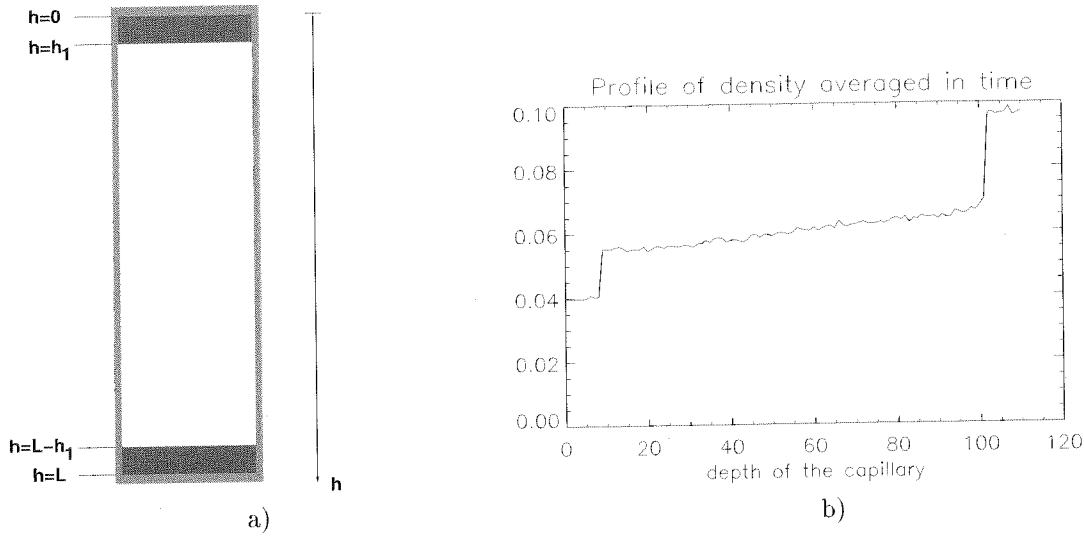

Fig. 4. — a) Drawing of the capillary used in Poiseuille flow experiment. Solid walls are in light grey and fixed density regions are in dark grey. b) Measured density profile on a 120×48 lattice for model C. Gas densities $\rho_1 (< \rho_G)$ and $\rho_2 (= \rho_G)$ are fixed in the ranges $[0, h_1] = [0,\ 9]$ sites and $[L - h_1, L] = [102,\ 112]$ sites respectively. A pair of density jumps appears between 9 and 10 sites and between 101 and 102 sites. Note that top and bottom walls densities are not displayed.

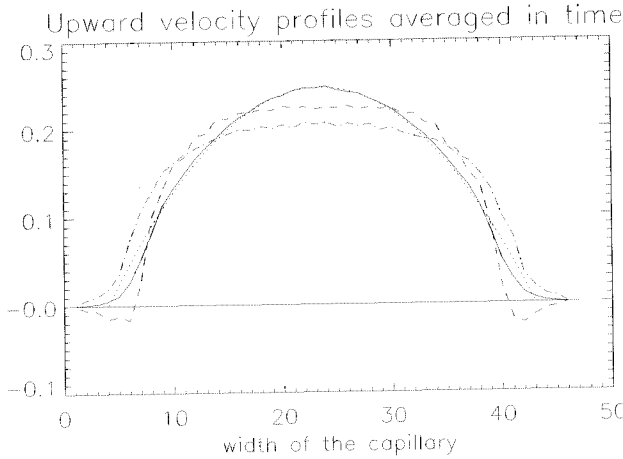

Fig. 5. — Upward velocity profiles in the gas region on a 120×48 lattice for model C. The different line ornaments correspond to different heights through the capillary. Dotted-dashed, solid and dashed profiles were measured at heights h equal to 16, 50 and 100 sites respectively. We drew the reference mark of zero velocity. The profiles on top and bottom of the capillary are of a Blasius type while the profile on the central region of the channel is well fitted with a Poiseuille velocity solution represented by the dotted line. Notice how the liquid films formed along the vertical walls and of about 3 sites wide affect the shape of the velocity profiles. Note particularly that a counter flow occurs in the films at the bottom of the capillary.

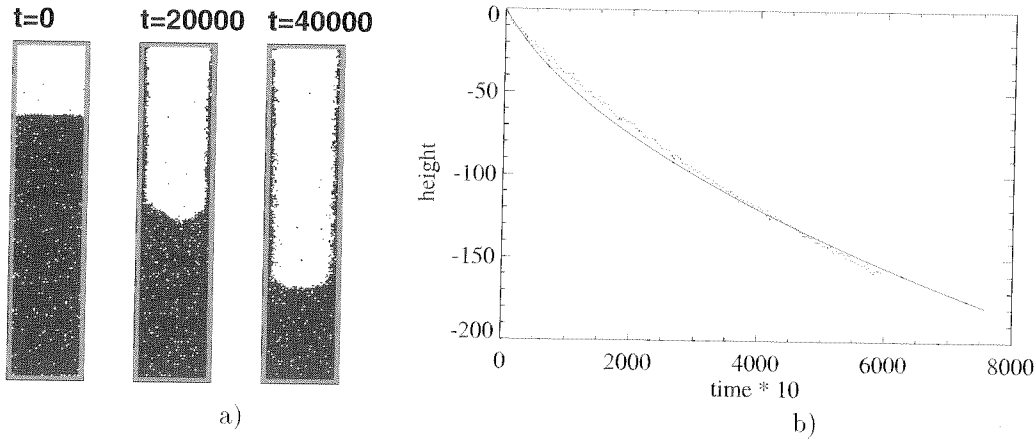

Fig. 6. — a) Evaporation in a capillary channel on a 240 × 48 lattice. The image is generated as in Figure 2. (b) Position of meniscus as a function of time. The solid lines represents the theory and dots are numerical data. Viscous effects slow down evaporation as time progresses.

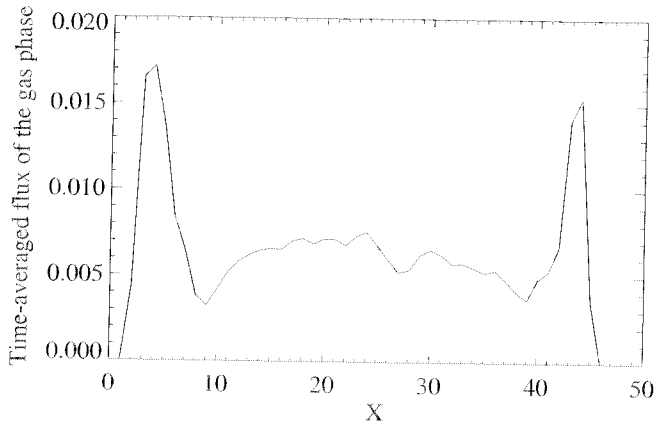

Fig. 7. — Flux of the particles in the gas region, averaged in time and for $16 \leq z \leq 32$ for Model A. Notice the important flux in the wetting layers on the side of the channel. In lattice units, the flux is the number of particles per time step.

The height of the liquid column diminished at a rate which depends on the gas density at the interface and on viscous properties in the gas. Figure 6 shows a computer-generated image of this numerical experiment as well as a plot of the position $h_0 - h(t)$ of the meniscus. Both Models A and C were used for these experiments, although Figure 6 shows the result for Model A. Assuming Poiseuille flow in the gas phase it is easy to obtain a theory, analogous to a classical Darcy scale theory, that predicts the rate at which the position $h(t)$ of the meniscus will vary. We obtain a classical Poiseuille flow solution from the Navier-Stokes equations (1) and (2). The mass conservation equation (7) gives the velocity of the interface $V_\mathrm{I} = \mathrm{d}h/\mathrm{d}t$. The pressure gradient in the capillary is $A = c_\mathrm{s}^2(\rho_\mathrm{f} - \rho_\mathrm{i})/h(t)$. In this equation ρ_i is the density just above the meniscus (which differs from ρ_G because of the density jump effect) and ρ_f is the density just below the top of the capillary at $z = 0$ where the density is imposed (ρ_f differs

from ρ_1 when a jump is present). We recall that $c_s^2 = \mathrm{d}p/\mathrm{d}\rho$ is the compressibility of the gas phase. The result is

$$h(t)^2 = h_0^2 + \frac{\rho_i c_s^2 R^2 (\rho_f - \rho_i)}{\eta_G (\rho_i - \rho_L)} t, \tag{10}$$

and it also appears in Figure 6b. It has a qualitative agreement with simulations. The difference comes from an important flow in the wetting films that transports mass in parallel with the Poiseuille flow.

This film flow is clearly seen in Figure 7 which shows the space and time-averaged flux of particles in a section of the channel. The large transport in the wetting films is obvious. Just as wetting films are a microscopic feature of the liquid-gas model the flow in these films is also a microscopic property. It is not described by the hydrodynamical equations of Section 2.1.2. Although this flow would become negligible for larger scale experiments, it is significant for the range of channel widths we used. It is also more important for Model A than for Model C. The difference originates in the higher gas density in Model C, which tends to let the Poiseuille flow in the gas phase transport more mass.

3. Dynamical Simulations in Porous Media

Our 2-D model of a porous medium consists of networks of capillaries constructed by placing square solid obstructions on the two-dimensional triangular lattice. This model is inspired by similar models used in experiments [25].

A representative simulation of evaporation in porous media is shown in Figure 8. The lattice contained 480 by 480 sites. Each direction could accommodate 12 square obstructions. Channel widths were randomly distributed between 16 and 32 lattice units in the horizontal direction. We had approximately the same distribution in the vertical direction. The simulation was initiated by filling the porous medium entirely with liquid except for a few of the upper rows. "Evaporation" was performed at the top of the model as described in Section 2.2 with $\rho_1 = 0$. The capillary number in the simulation was $\mathrm{Ca} \simeq 10^{-2}$. With larger ρ_1 as in Section 2.4 slower evaporation and smaller capillary numbers would occur but the simulations would be exceedingly long.

Animated visualizations or "movies" of the simulations showed a complex and interesting behavior. A striking feature was the abrupt progression of the liquid through narrow pores. This behavior is qualitatively similar to the bursts described by Shaw [7]. The menisci were observed to stop either at the entrance or the exit of a pore. We have studied in detail this phenomenon of pinning by performing additional simulations involving the single pore shown in Figure 2. They confirm that because of capillary effects the pressure jumps at the entrance and exit of a square pore throat.

We also noticed that the recession of the front slows down during the simulation. Indeed, the pressure gradient between the top of the model and the evaporating front decreases. This in turn decreases the flow of gas as in the single channel experiments of Section 2.4.

For the hexagonal grain geometry, bursts similar to those observed on the square lattice were seen. The details of the bursts, however, were different: the meniscus could sweep in one burst all of the 6 large pores surrounding a single small hexagonal grain, while for square grains the bursting involved only one or two pores. An example of evaporation with a large porous medium and hexagonal grains is shown in Figure 9. The interface becomes more irregular than in Figure 8.

The lattice-gas method allows for an easy implementation of various boundary conditions, including simple models of fractured media. For instance Figure 10 shows a model with a

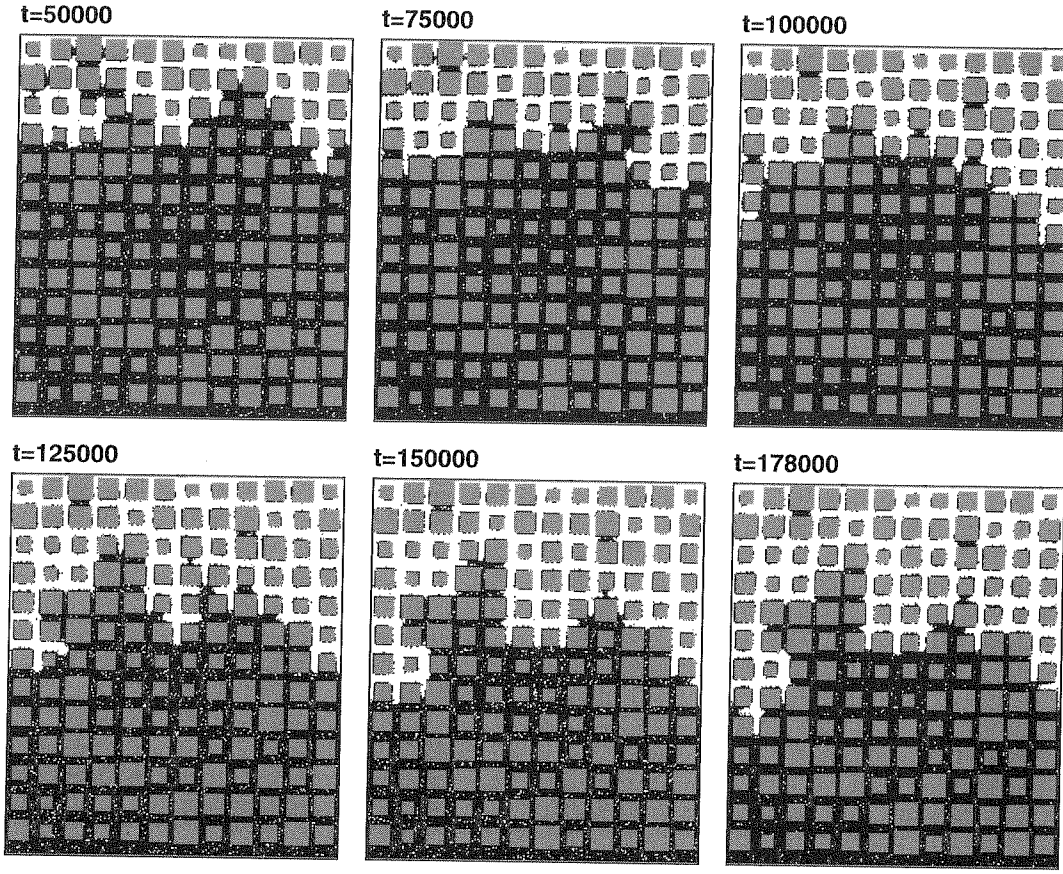

Fig. 8. — Evaporation on a 480 × 480 lattice with Model A, $g_w = 4$

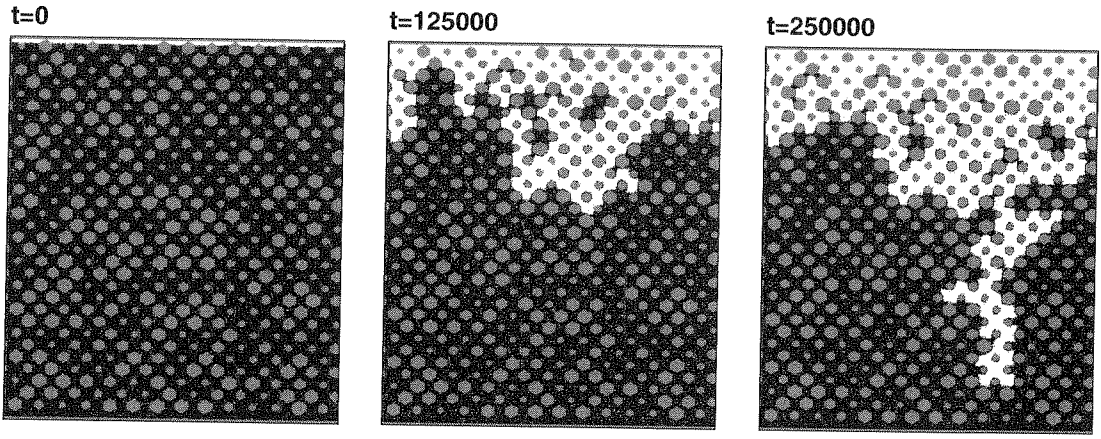

Fig. 9. — Evaporation on a 480 × 480 lattice with Model A, $g_w = 2$ and hexagonal grains.

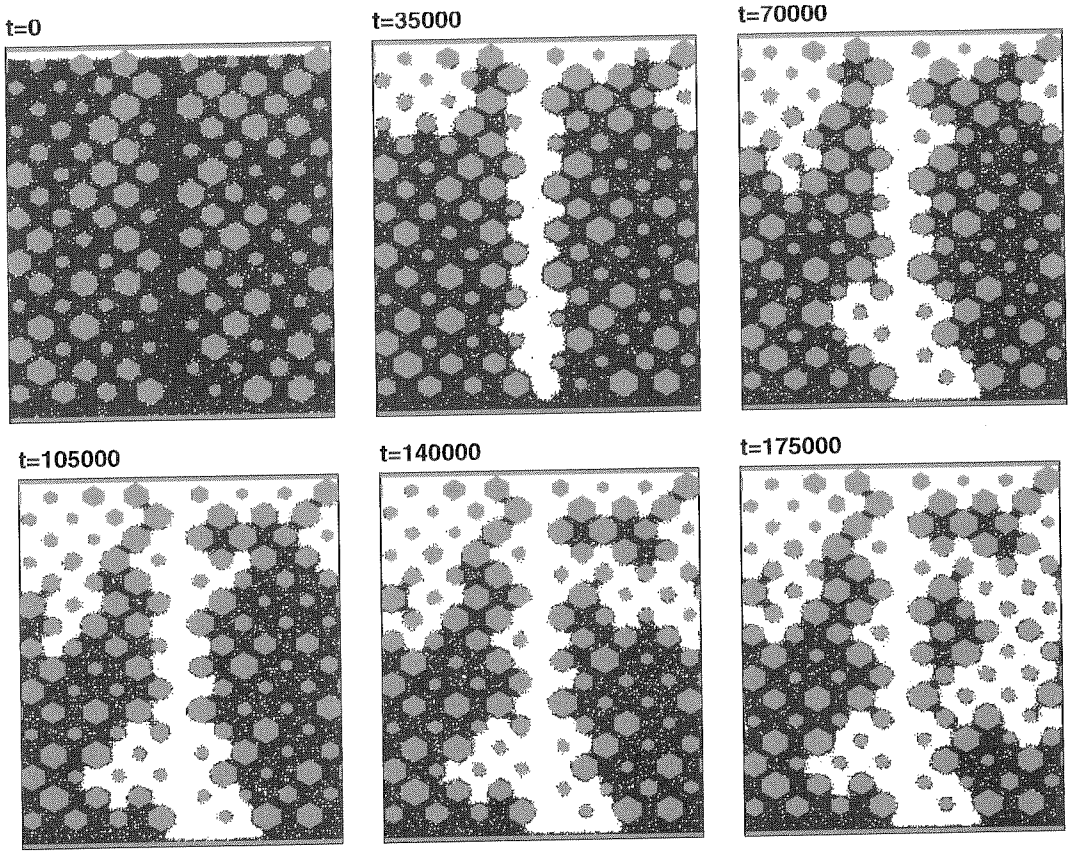

Fig. 10. — Evaporation on a 240 × 240 lattice with hexagonal grains (Model A with $g_w = 2$ was used). Notice how the area of high porosity empties first.

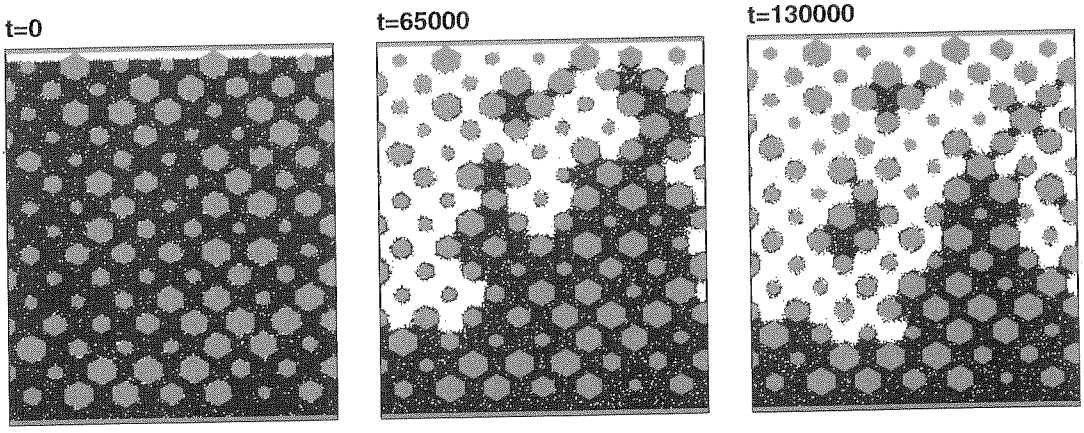

Fig. 11. — Same as Figure 10 without the area of high porosity.

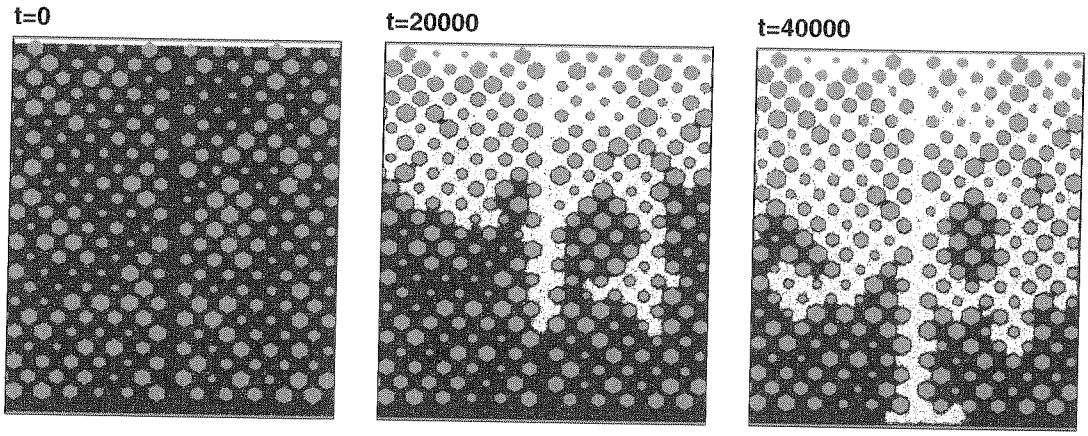

Fig. 12. — Evaporation on a 480 × 480 lattice with hexagonal grains and Model C with $g_w = 2$. An area of high porosity is introduced as in Figure 10. This areas empties more rapidly than the surrounding porous medium. The invasion in this area is comparatively slower than with Model A.

region of high porosity in the middle of the domain. The simulation is realized on a 240 by 240 lattice with a distribution of channel widths between 12 and 24 lattice units. The distribution of the channel widths for the area of high porosity is between 20 and 50 lattice units. When the high porosity area is absent a more regular final stage was observed (see Fig. 11). A simulation with Model C and a larger "fractured" lattice is shown in Figure 12.

Another frequently observed effect in our simulations with Model C is the appearance of gas bubbles inside the liquid phase; *i.e.*, cavitation. (This effect is not in the figures included here because of lack of space.) It occurs in the small pores. It is a consequence of the Gibbs-Thomson relation (8) for P_L, which implies that the liquid pressure is negative for small radii. Such phenomena have also been seen in laboratory experiments (S. Bories, personal communication).

4. Discussion and Conclusion

We have introduced a new model for the simulation of isothermal evaporation in solid matrices. The model has been validated in this paper by static and dynamic experiments. The wetting properties which are new to the model have in particular been tested in several ways. As an example of the possible uses of the liquid-gas model we have performed evaporation experiments on square and hexagonal matrices. These simulations show qualitative features similar to those observed in real experiments.

An unexpected result of our dynamical tests was the transport of flow in thin liquid films. Since our films are very thin, of the order of the interaction range, it is difficult to explain this motion in the framework of continuum mechanics. However it is possible that such a motion actually contributes to water transport in very thin capillaries.

As our work is mostly methodological it is useful to consider the limitations of the modelling presented in this paper. One simplifying assumption which is easy to lift is the absence of gravity. Gravity can easily be simulated as has been done with the liquid-gas model in other studies [22]. Here, thinking on the scale of a few real pores gravity is irrelevant, although it may become relevant in laboratory scale porous media [26].

There are more serious limitations related to the nature of the liquid gas model. The liquid phase should be at rest to allow for correct jump conditions on the interface. The Reynolds number of the gas phase should be small to avoid difficulties with the non-linear term of the Navier-Stokes equations. Finally we are limited to isothermal problems with a single species in both liquid and vapor states. This last limitation is probably the most important one for applications to natural evaporation phenomena.

We expect that further progress in lattice-gas methods will alleviate some of the limitations of the liquid-gas model. Already models extended to three dimensions of space have been proposed and used to simulate evaporation [27]. A better theoretical modelling of the interaction has allowed theoretical estimates of the surface tension and equilibrium pressures [27]. A still better understanding of the workings of the interaction may allow to obtain further variants of the models with the correct nonlinearity in the Navier-Stokes equations. The addition of more species is also a potential improvement. However we see no clear prospect for the addition of thermal effects.

One may also legitimately ask what advantages the use of the lattice-gas method offers compared to competing methods for the simulation of interfacial flow in porous media. Although the lattice-gas method bears some similarities with network models such as percolation methods, lattice-gas methods contain more physics (for example, the Navier-Stokes equations), and thus allow one to reach more fundamental conclusions about the nature of porous flow. For example, a study of evaporation between the liquid film scale and a macroscopic, many-pore scale is a problem of intrinsic interest that is inaccessible to the more specialized percolation methods. However the results in this paper do not prove that the lattice-gas method has a compelling advantage in speed or ease of use for the solution of the Stokes equations. More classical methods for the simulation of flows with interfaces exist [28,29]. On the positive side the lattice gas has an advantage in the ease with which boundary conditions on solid grains are implemented. In classical finite element or finite volume methods, complex boundary conditions lead to cumbersome grid generation.

Beyond this technical advantage in dealing with boundary conditions the clearest benefit we perceive now in lattice-gas simulations lies in their additional microscopic realism. For instance the motion in the liquid films seems to be a real microscopic effect at very small scale although the modelling of the wall-particle attraction is very crude. The presence of density jumps may also be an interesting kinetic effect, albeit presently misunderstood. On the other hand there are obvious difficulties with the lattice gas formulation such as the present impossibility to simulate real water/air conditions and in particular realistic capillary numbers. We do not know however how difficult it would be to devise a "classical" method free of that problem.

Another comparison should be made with other lattice-gas methods such as the "immiscible lattice gas" [8]. Although the two models allow superficially for similar types of pore-scale studies they differ in many respects. This becomes obvious with the results of the validation experiments in this paper. The liquid-gas model principally offers the possibility of a change of phase. This possible phase change modifies the equations at the Navier-Stokes level and leads to the Gibbs-Thomson relations (8). Another important difference is the occurrence of asymmetrical densities in the liquid-gas model, which have never been introduced in immiscible lattice gases where phase separation manifests itself as the separation of two species of particles into separate regions. Finally the longer-range interaction in liquid-gas models allows for discernible wetting layers, though long-range interactions in immiscible lattice gases could (but have never been shown to) yield similar results.

Another question which is not yet resolved is whether pore scale modelling will be useful to improve, or provide parameters for, the equations describing the physics at a much larger scale. It is probably too early to answer such a question. To be quantitatively comparable with the

natural situations that larger scale models attempt to describe microscopic simulations should be performed in 3D, and with several species. A preliminary 3D lattice gas simulation has already been performed [27]. One of the potential interests of a 3D simulation is the possibility of having a complex film flow connecting the saturated regions to the outer boundary of the medium.

These more realistic studies will be possible with new lattice-gas models. In the meantime, with the models in mostly their present form, it is possible to investigate many basic physical processes. The flow in thin films should be more extensively studied. With longer-range wall potentials the thickness of the wetting films could be increased. Variation of the wall potential could also tune the wetting properties which appear crucial in both static and dynamic aspects of evaporation.

Acknowledgments

This work was supported in part by NSF Grant 9218819-EAR, by the sponsors of the MIT Porous Flow Project, and by NATO Travel Grant 10756. C. Appert, D.H. Rothman, and S. Zaleski benefited from mutual visits to their home institutions for which they thank École Normale Supérieure (Paris), CNRS, the CNES microgravity programme, and NATO.

References

[1] Sheidegger A.E., The Physics of Flow Through Porous Media (Macmillan Company, New York, 1960).
[2] Bear J., Dynamics of Fluids in Porous Media (Dover Publications, New York, 1972).
[3] Feder J., Fractals (Plenum Press, New York, 1988).
[4] Richter F.M. and McKenzie D.P., *J. Geol.* **92** (1984) 729-740.
[5] Bensimon D., Kadanoff L.P., Liang S., Shraiman B.I. and Tang C., *Rev. Mod. Phys.* **58** (1986) 978.
[6] Quenard D., Adsorption et transfert d'humidité dans les matériaux hygroscopiques. Approche du type percolation et expérimentation, PhD thesis, Institut National Polytechnique de Toulouse (1989).
[7] Shaw T.M., *Phys. Rev. Lett.* **59** (1987) 1671.
[8] Rothman D.H., *J. Geophys. Res.* **95** (1990) 8663.
[9] Gunstensen A.K. and Rothman D.H., *J. Geophys. Res.* **98** (1993) 6431-6441.
[10] Frisch U., Hasslacher B. and Pomeau Y., *Phys. Rev. Lett.* **56** (1986) 1505-1508.
[11] Frisch U., d'Humières D., Hasslacher B., Lallemand P., Pomeau Y. and Rivet J.-P., *Complex Systems* **1** (1987) 648.
[12] G.D. Doolen, Ed., Lattice Gas Methods for Partial Differential Equations (Addison-Wesley, 1991).
[13] Benzi R., Succi S. and Vergassola M., *Phys. Rep.* **222** (1992) 145-197.
[14] Rothman D.H. and Zaleski S., *Rev. Modern Phys.* **66** (1994) 1417-1479.
[15] Appert C. and Zaleski S., *Phys. Rev. Lett.* **64** (1990) 1.
[16] Appert C. and Zaleski S., *J. Phys. II France* **3** (1993) 309-337.
[17] Appert C., Rothman D.H. and Zaleski S., *Physica D* **47** (1991) 85-96.
[18] Appert C., d'Humières D. and Zaleski S. *C. R. Acad. Sci. Paris* **316** (1993) 569-574.
[19] Rothman D.H. and Keller J., *J. Stat. Phys.* **52** (1988) 1119.

[20] Rocard Y., Thermodynamique, 2ème édition (Masson, Paris, 1967).
[21] Churaev N.V., *Rev. Phys. App.* **23** (1988) 975.
[22] Di Pietro L.B., Melayah A. and Zaleski S., *Water Resources Res.* **30** (1994) 2785-2792.
[23] d'Humières D. and Lallemand P., *Complex Systems* **1** (1987) 599-632.
[24] Schlichting H., Boundary Layer Theory, Chap. 9 (McGraw Hill, New York, 1979).
[25] Lenormand R., Zarcone C. and Sarr A., *J. Fluid Mech.* **135** (1983) 337.
[26] Puiggali J.R., Quintard M. and Whitaker S., *Drying Technol.* **6** (1988) 601-629.
[27] Appert C., Pot V. and Zaleski S., Liquid-gas models on 2D and 3D lattices, In Fields Institute Communications editor, *Pattern Formation and Lattice-Gas Automata*, volume 6 (American Mathematical Society, 1996) pp. 1-11.
[28] Hyman J.M., *Physica D* **12** (1984) 396-407.
[29] Lafaurie B., Nardone C., Scardovelli R., Zaleski S. and Zanetti G., *J. Comp. Phys.* **113** (1994) 134-147.